Energy & Environmental Science

Accepted Manuscript

ROYAL SOCIETY OF CHEMISTRY

www.rsc.org/ees

Photosynthesis of Formate from CO_2 and Water at 1% Energy Efficiency via Copper Iron Oxide Catalysis

Unseock Kang,[1] Sung Kyu Choi,[2] Dong Jin Ham,[3] Sang Min Ji,[3] Wonyong Choi,[4] Dong Suk Han,[5] Ahmed Abdel-Wahab,[5] and Hyunwoong Park[1,*]

[1]*School of Energy Engineering and* [2]*Department of Physics, Kyungpook National University, Daegu 702-701, Korea*

[3]*Energy Laboratory, Materials R&D Center, Samsung Advanced Institute of Technology, Samsung Electronics Co., LTD, Yongin 446-712, Korea*

[4]*School of Environmental Science and Engineering, POSTECH, Pohang, 790-784, Korea*

[5]*Chemical Engineering Program, Texas A&M University at Qatar, Education City, Doha, P.O. Box 23874, Qatar*

Submitted to

Energy & Environmental Science

Revised

(June 20, 2015)

*To whom correspondence should be addressed (H. Park)
Tel: +82-53-950-8973; Fax: +82-53-950-8979
E-mail: hwp@knu.ac.kr

Abstract

Solar conversion of carbon dioxide and water to value-added chemicals remains a challenge. A number of solar-active catalysts have been reported but still suffer from low selectivity, poor energy efficiency, and instability, and fail to drive simultaneous water oxidation. Herein, we report $CuFeO_2$ and CuO mixed p-type catalysts fabricated via a widely employed electroplating of earth-abundant cupric and ferric ions followed by annealing under atmospheric air. The composite electrodes exhibited onset potentials at +0.9 V vs. RHE in CO_2-purged bicarbonate solution and converted CO_2 to formate with over 90% selectivity under simulated solar light (Air Mass 1.5, 100 $mW \cdot cm^{-2}$). Wired $CuFeO_2$/CuO photocathode and Pt anode couples produced formate over 1 week at a solar-to-formate energy conversion efficiency of ~1% (selectivity >90%) without any external bias while O_2 was evolved from water. Isotope and nuclear magnetic resonance analyses confirmed the simultaneous production of formate and O_2 at the stand-alone couples.

Graphical Abstract

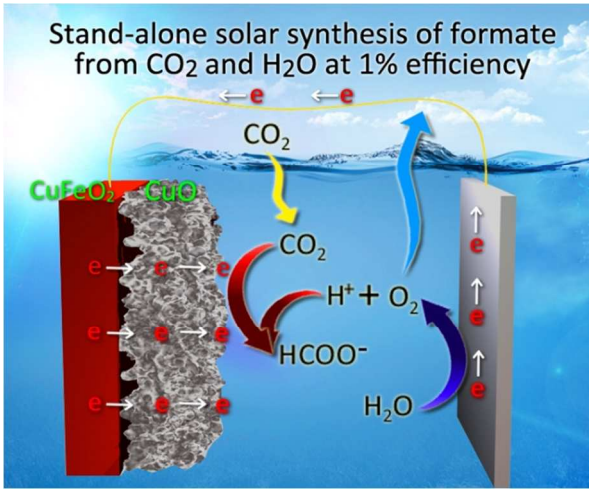

Solar CO_2 recycling has received wide attention primarily to address global CO_2 emission and to convert CO_2 and water to value-added chemicals.[1-3] Despite a long research history over the past four decades,[4,5] the technology remains in an early stage, with low CO_2 conversion efficiency and selectivity. CO_2 is highly stable and has limited solubility in water, and its reduction requires multiple proton-coupled electron transfers, resulting in a range of carbon intermediates (C1 – C3)[2,6] as well as a larger amount of H_2 over CO_2 conversion products.[7-9]

For the realization of solar CO_2 recycling, the system of interest should be operated sustainably, which requires the development of not only energy-efficient and cost-effective materials but also stand-alone, complete reaction processes (CO_2 reduction and water oxidation) operating for long periods without any external bias.[10-12] A range of semiconductors (mostly p-types) have been studied for CO_2 conversion, including GaP,[4] InP,[5] GaAs,[13] Si,[8,14] Cu_2O,[15-18] and $CuFeO_2$,[19,20] all of which have narrow bandgaps (E_g) and sufficient Fermi levels (E_F) capable of reducing CO_2. Although promising, these materials inherently require potential biases to drive the CO_2 reduction reaction and compete with other metallic electrodes,[21] whereas complete reactions (CO_2 reduction and water oxidation) have been rarely demonstrated due to large overpotentials. Photocathode-photoanode couples have been demonstrated to operate,[11] yet the syntheses of materials are complicated and the energy conversion efficiency is low (max. 0.14%).

We have searched for high-efficiency, low-cost, and scalable p-type materials and found that $CuFeO_2$ and CuO mixed materials meet all requirements. To our surprise, this material converted CO_2 to formate with selectivity greater than 90% over 1 week and simultaneously produced molecular oxygen via water oxidation when simply wired to an inert anode (Pt foil) without any external bias under circum-neutral pH. The solar-to-formate (STF) energy efficiency was in the range of 0.7 – 1.2%, which is the highest reported value and comparable to the

efficiency of photosynthesis occurring in most plants. For comparison, $CuFeO_2$,[19,20] CuO,[16] and even Cu_2O[15] were fabricated; however, their efficiencies for formate production were much lower, and no oxygen was evolved.

Fig. 1a shows the XRD patterns of four p-type oxide samples ($CuFeO_2$/CuO, Cu_2O, CuO_2, and $CuFeO_2$) that were obtained via electrodeposition on conducting glass electrodes (FTO) at −0.36 V_{SCE} for 2 h and calcination at 650 °C for 3 h under air or Ar atmospheres. In the presence of aqueous cupric ions (Cu^{2+}) alone in the plating solution, electrodeposition followed by calcination under air and argon atmospheres created CuO and Cu_2O, respectively. In the presence of cupric ions and ferric ions (Fe^{3+}) together, copper and iron were co-electrodeposited and transformed into pure $CuFeO_2$ and mixed $CuFeO_2$/CuO oxides when annealed under Ar and air atmospheres, respectively. With the mixed $CuFeO_2$/CuO sample, most identified XRD phases originated from CuO, whereas well-defined phases of $CuFeO_2$ (e.g., 012 and 024) were observed. No peaks related to other oxides (e.g., $CuFeO_{2+\delta}$, $CuFe_2O_4$, or Fe_3O_4) were observed,[22] which indicates that calcination in the presence of atmospheric air segregates Fe species and oxidizes Cu(I) to Cu(II). XPS analysis showed that the $Cu2p_{3/2}$ bands of the samples annealed under Ar atmosphere have the same binding energy at 931.4 eV (Fig. 1b), coinciding to Cu(I) and supporting the formation of Cu_2O and $CuFeO_2$. With the samples obtained under air atmospheres, $Cu2p_{3/2}$ bands shifted to high binding energy (932.6 - 932.7 eV) due to the oxidation of Cu(I) to Cu(II). In addition, the copper binding energy of $CuFeO_2$/CuO was ~0.2 eV smaller than that of CuO, indicating that Cu(I) and Cu(II) coexist in the mixed phase while the latter is more abundant. The $Fe2p_{3/2}$ bands of $CuFeO_2$ and $CuFeO_2$/CuO samples displayed the same binding energy at 710.5 eV (Fig. 1b inset), which were assigned to Fe(III).[23] Characterization via XRD and XPS, therefore, verifies that the simultaneous electrodeposition of Cu(II) and Fe(III) and

subsequent oxidative annealing create CuO and $CuFeO_2$ bicrystallines preferentially.

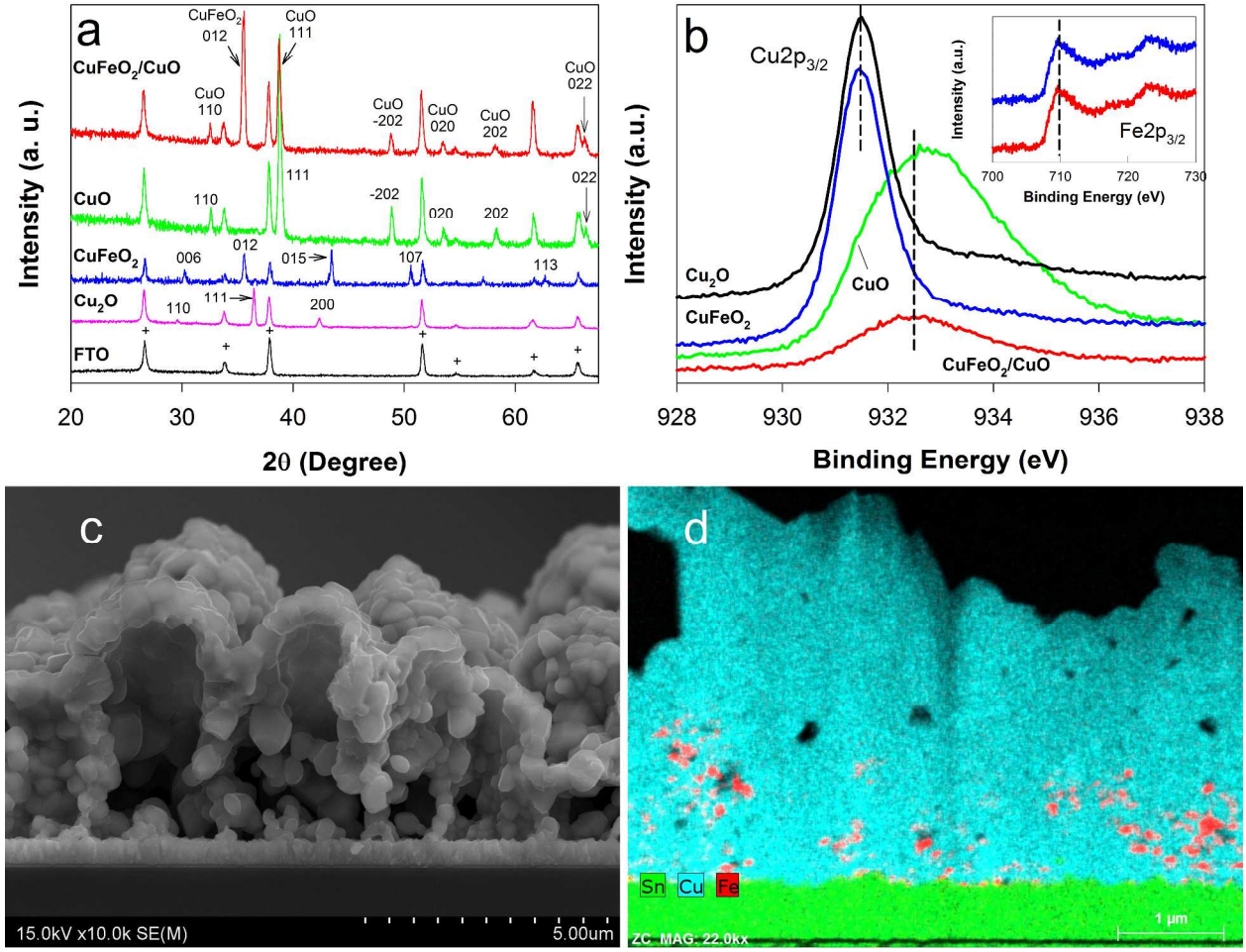

Fig. 1. Surface characterization of $CuFeO_2$/CuO, CuO, $CuFeO_2$, and Cu_2O films electrodeposited on FTO for 2 h followed by calcinations under air or Ar atmospheres (see text and *Supporting Information* for detailed synthetic conditions): (a) XRD (+ originating from FTO); (b) XPS Cu2p bands (inset: Fe2p bands); (c) cross-sectional TEM images of $CuFeO_2$/CuO (see *Supporting Information* for other images); (d) EDX elemental mapping for the cross-section of $CuFeO_2$/CuO (green: Sn, blue: Cu, red: Fe).

The samples showed morphologies of double-layered structures. $CuFeO_2$/CuO had a ca. 500-nm-thick underlayer and 4 - 5-μm-thick hollow overlayer (Fig. 1c). The thickness and morphology of the underlayer were very similar to those of the other three oxides (Fig. S1a – c in *Supporting Information*), suggesting a similar deposition mechanism and kinetics. Our

preliminary study of the growth mechanism of a $CuFeO_2$/CuO film showed that the underlying thin film grows to ~500 nm in 10 s and does not further grow for the next 300 s. Uniformly distributed porous bumps of ~500 nm with an inter-distance of ~500 nm were then created on the underlayer, being transformed into the overlying porous structures in 600 s and finally 2 – 3-μm-sized aggregates. TEM/EDX elemental mapping of the cross-section of a $CuFeO_2$/CuO film showed the distribution of elemental Fe within a thickness of ~1.5 μm from the bottom (Fig. 1d). However, elemental mapping of the top of the $CuFeO_2$/CuO film showed the co-presence of Cu and Fe in an atomic ratio of 1.4 (Fig. S2a). For comparison, $CuFeO_2$ exhibited a Cu and Fe atomic ratio of 1.06 (Fig. S2b). $CuFeO_2$ appeared to be located in the bottom regions, whereas CuO was uniformly distributed throughout the entire region.

The photoelectrochemical responses of as-prepared $CuFeO_2$/CuO electrodes were examined in 0.1 M bicarbonate solution purged with different gases (N_2, CO_2, and O_2). With N_2-purging, the electrodes generated cathodic photocurrents from ca. +0.86 V_{RHE} (Fig. S3), whereas O_2-purging slightly increased cathodic photocurrent generation due to faster interfacial electron transfer to O_2 compared to water reduction with N_2-purging.[19] When CO_2 was purged, the photocurrent generation was further enhanced, and the onset potential (E_{on}) was anodically shifted to +0.95 V_{RHE} (Fig. 2a), which suggests that the $CuFeO_2$/CuO photoelectrode could be effective for not only O_2 reduction but also, more significantly, CO_2 reduction. For comparison, CuO, Cu_2O, and $CuFeO_2$ electrodes were also tested in CO_2-purged bicarbonate solution (Fig. 2a). CuO exhibited E_{on} of +0.73 V_{RHE} and insignificant dark current generation even at +0.3 V_{RHE}. However, CuO showed a cathodic peak at +0.65 V_{RHE} due to Cu^{2+} reduction ($E°(Cu^{2+/+})$ = +0.159 V; $E°(Cu^{2+/0})$ = +0.340 V). $CuFeO_2$ (Fig. 2a) and Cu_2O (Fig. S4) showed large dark current generations and unstable photoresponses. Accordingly, only $CuFeO_2$/CuO was found to

be the most suitable candidate in terms of E_{on}, magnitude of photocurrent generation, and photoelectrochemical stability.

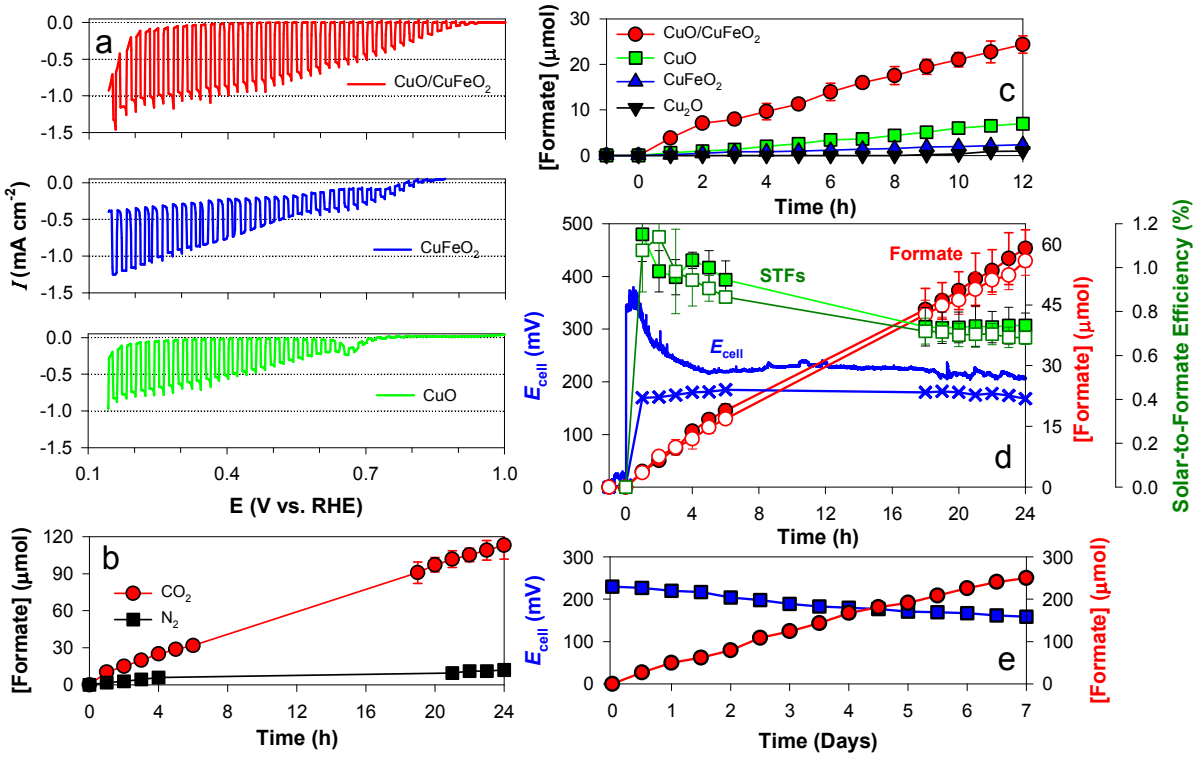

Fig. 2. (a) Comparison of light-chopped linear sweep voltammograms for $CuFeO_2$/CuO, $CuFeO_2$, and CuO electrodes in CO_2-purged aqueous bicarbonate (0.1 M) solution. (b) Time-profiled formate productions with $CuFeO_2$/CuO electrodes at +0.15 V_{RHE} in bicarbonate (0.1 M) solutions purged with CO_2 or N_2 (PEC-1). (c) Comparison of time-profiled formate productions with open-circuited $CuFeO_2$/CuO, $CuFeO_2$, and CuO, and Cu_2O electrodes in CO_2-purged bicarbonate (0.1 M) solution (PEC-2). No potential biases were applied, and only open-circuit potentials (E_{ocp}) were recorded with a potentiostat during irradiation. (d) Time-profiled changes in cell voltage (E_{cell}), simultaneous production of formate, and solar-to-formate (STF) energy conversion efficiencies with wired $CuFeO_2$/CuO and Pt foil couples in CO_2-purged bicarbonate (0.1 M) solutions (PEC-3 and 4). In this two-electrode system, the $CuFeO_2$/CuO and Pt electrodes faced with a distance of ~ 3 mm, and E_{cell} was recorded using a potentiostat (solid blue line and filled symbols; PEC-3) or a multimeter (crossed blue line and open symbols; PEC-4). (e) Changes in E_{cell} and formate production with a wired $CuFeO_2$/CuO and Pt couple in CO_2-purged bicarbonate (0.1 M) solutions (PEC-4). A simulated light (AM 1.5; 100 $mW \cdot cm^{-2}$) irradiated sample electrodes through FTO. See Scheme S1 in the *Supporting Information* for PEC-1, 2, -3, and -4 setups.

The performance of $CuFeO_2$/CuO for photoelectrochemical CO_2 conversion was tested in CO_2-purged 0.1 M bicarbonate electrolyte under irradiation of AM 1.5G (100 $mW \cdot cm^{-2}$). Upon irradiation at a potential bias (E_{bias}) = +0.15 V_{RHE} (PEC-1), formate was produced linearly at ~5 $\mu mol \cdot h^{-1}$ over 24 h with CO_2-purging (Fig. 2b). With N_2-purging (i.e., minimized aqueous CO_2), formate production significantly decreased to ~0.5 $\mu mol \cdot h^{-1}$ due to reduction of bicarbonate to formate. During the course of this potential-biased photoelectrocatalysis, other carbon compounds (CO, HCOH, CH_3OH, and C1-C4 hydrocarbons) were not detected or, even if produced, below detection limits. However, $CuFeO_2$/CuO could produce formate even at +0.35 V_{RHE} at ca. 2.5 $\mu mol \cdot h^{-1}$ (Fig. S5). Owing to dark currents at $E_{bias} < +0.4$ V_{RHE} (Fig. 2a), formate was electrochemically produced; however, the yields were 3 – 4% of those obtained photoelectrochemically (e.g., 0.1 $\mu mol \cdot h^{-1}$ at E_{bias} = +0.35 V_{RHE}). Notably, H_2 production was not observed in the potential range of +0.15 and +0.35 V_{RHE} despite a similar reduction potential as $E°(CO_2/HCOOH)$ (0.026 V_{RHE}),[24] which is attributed presumably to the favored sorption of CO_2 and/or H^+ on the surface followed by predominant proton-coupled electron (e.g., $2e^-$, $1H^+$) transfer. A detailed mechanism study is underway.

More importantly, this electrode was found to operate even in the absence of applied biases in the typical three-electrode system (PEC-2). Upon irradiation, formate was continuously produced at ca. 2 $\mu mol \cdot h^{-1}$ over 12 h in open-circuit potential (E_{ocp}) mode (Fig. 2c). Simultaneously, E_{ocp} was increased from ca. +0.55 to +0.8 ~ 0.83 V_{RHE} (Fig. S6), which was ~150 mV negative of the E_{on} value due to charge recombination (Fig. 2a). CuO, Cu_2O, and $CuFeO_2$ were also found to operate under the same condition, yet formate production rates were much lower than that of $CuFeO_2$/CuO.

For benchmark efficiency,[25] a $CuFeO_2$/CuO electrode was directly wired to a Pt foil electrode in a single cell with CO_2-purged bicarbonate electrolyte (PEC-3 and 4), and the cell potentials (E_{cell}) were recorded using a potentiostat (PEC-3) or a multimeter (PEC-4) while produced formate was intermittently quantified (Fig. 2d). Upon irradiation, E_{cell} increased from ~10 mV to ~350 mV and stabilized at ~220 mV in 5 h, while formate was continuously produced to ~60 μmol in 24 h (2.5 $\mu mol \cdot h^{-1}$). Both analytical methods (PEC-3 and 4) were found to yield similar results. With this two-electrode system, the STF efficiency was 1 - 1.2% for the initial period of 5 h and then stabilized to ~0.7% for the following hours. This efficiency is approximately eight-fold higher than that reported previously.[11] In addition, formate production continued over 1 week and reached ~250 μmol in day 7, while E_{cell} gradually decreased from ~230 mV to ~170 mV (Fig. 2e). The electrolyte was analyzed with ICP-MS after the long-term test; however, neither Fe nor Cu ions were found. However, the partial reductions of Cu(II) to Cu(I) as well as Fe(III) to Fe(II) were observed. A more detailed study is underway. Although marginal, the decrease in formate production rate and E_{cell} was attributed to the oxidation of accumulated formate at the Pt anode (Fig. S7 and *see below*). This high STF efficiency with durability over a week has never been reported. Taking into account the earth abundance of photoelectrode components (Cu and Fe) and the simplicity of electrode synthesis (electrodeposition followed by annealing at relatively low temperature in the presence of atmospheric air, which is achievable in any undergraduate laboratory and with undergraduate skill), the application of this electrode to solar CO_2 conversion is highly promising.

The faradaic efficiency for formate production was estimated by applying constant cathodic currents (–0.2 and –0.3 mA) to $CuFeO_2$/CuO electrodes. In the dark, no measurable amount of formate was produced, whereas, upon irradiation, formate was linearly produced over

12 h (Fig. 3a). The faradaic efficiencies were maintained at over 90%, while the potentials were nearly constant at +0.2 and –0.35 V_{RHE} under both galvanostatic conditions during the reactions. No H_2 evolution was observed. Increase in applied current to –0.5 mA resulted in a decrease in faradaic efficiency of 40 ~ 60% due to electrode damage (Fig. S8).

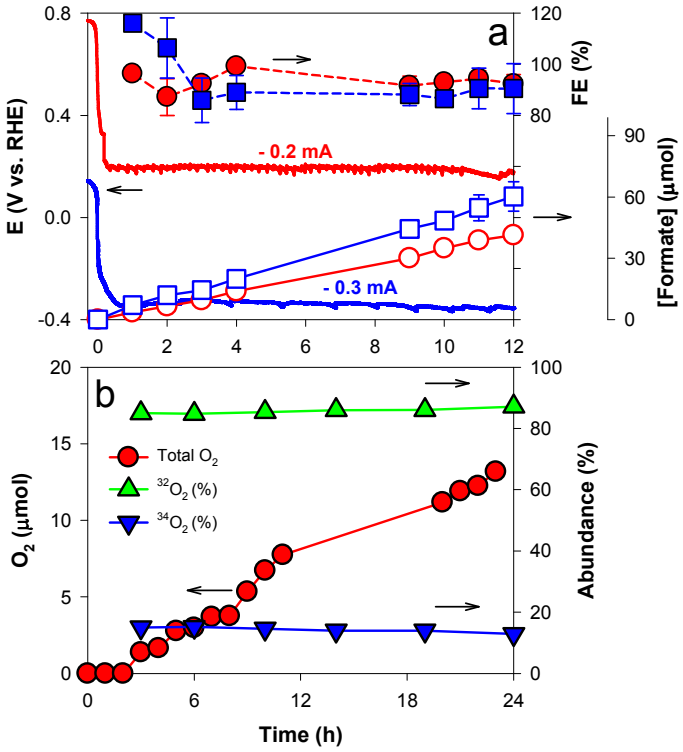

Fig. 3. (a) Time-profiled changes in potential of $CuFeO_2$/CuO (red and blue solid lines), production of formate (open symbols), and faradaic efficiency (closed symbols) under constant current (red circles: –0.2 mA; blue squares: –0.3 mA) with a three-electrode system in CO_2-purged bicarbonate (0.1 M) solution (PEC-1). (b) Oxygen evolution with a wired $CuFeO_2$/CuO and Pt foil couple (PEC-4) in ^{18}O-labeled water ($H_2{}^{18}O$, 20 vol. % in H_2O) as a solvent in which bicarbonate salt was dissolved (0.1 M) and CO_2 gas was purged for over 1 h prior to irradiation. The relative abundance of $^{32}O_2$ and $^{34}O_2$ was compared. A simulated light (AM 1.5G; 100 mW·cm^{-2}) irradiated $CuFeO_2$/CuO through FTO.

To identify the source of carbon in formate, a wired couple of $CuFeO_2$/CuO and Pt foil (PEC-4) was immersed in ^{12}C–bicarbonate solution through which $^{13}CO_2$ gas was purged. Upon irradiation, doublet ^{1}H-NMR shifts at ~8.57 and ~8.18 ppm ($^1J_{CH}$ = 195 Hz) that are associated

with the ^{13}C-formate gradually increased with time (Fig. S9a). Additionally, two ^{13}C-NMR shifts at 171 and 160.8 ppm were observed (Fig. S9b) that are associated with the presence of ^{13}C-formate and ^{13}C-bicarborate (natural abundance of ^{13}C ~1.1%), respectively. When $^{12}CO_2$ was purged through ^{13}C-bicarbonate solution, ^{1}H-NMR shifts at 8.26 ppm corresponding to ^{12}C-formate linearly increased (Fig. S9c). These NMR studies, therefore, verify that purged CO_2 is reduced to formate.

We also observed that molecular oxygen (O_2) was evolved with the wired $CuFeO_2$/CuO and Pt couple (PEC-4). O_2 production was relatively linear with irradiation time (Fig. 3b). We repeated the O_2-leaking test several times and confirmed that the observed O_2 amounts are reliable. Use of ^{18}O-labelled H_2O (20%) in aqueous bicarbonate solution further showed that 15 ~ 18% of the total headspace O_2 amount is $^{34}O_2$ (Fig. S10), verifying that O_2 is truly produced via the oxidation of water. However, the production ratios of formate and oxygen were higher than the theoretical value of 2 only if cathodic and anodic reactions (two- and four-electron-transfer processes, respectively) occur stoichiometrically (Fig. S11). This non-stoichiometry might be attributed partly to sluggish 4-electron water oxidation[26,27] and/or reduced water oxidation resulting from the competitive oxidation of accumulated formate (thermodynamically more feasible than water oxidation; see Fig. S7), limiting the overall STF efficiency. CuO and $CuFeO_2$ were also capable of producing formate from CO_2 in the two-electrode system (PEC-4; see Fig. S12). Nevertheless, CuO and $CuFeO_2$ were less effective than $CuFeO_2$/CuO because of low STF efficiencies (each and the sum of both), E_{cell}, and stability (Fig. 2d). Furthermore, no oxygen was evolved with these electrode systems.

In terms of the simultaneous production of formate and oxygen, these copper and iron mixed oxides should be a suitable candidate for artificial photosynthesis. The superior activity of

$CuFeO_2$/CuO electrode can be attributed to the heterojunction structure of $CuFeO_2$ and CuO that is capable of absorbing a broad band of the solar spectrum as well as inducing cascaded charge transfers at the interface.[16,28-30] Diffuse reflectance UV-Vis absorption spectra showed that the optical bandgap (E_g) of CuO particles is ~1.4 eV,[31] whereas $CuFeO_2$ appeared to have three primary band transitions at 1.05, 1.34, and 1.7 eV (Fig. S13). The first is the indirectly allowed transition,[32] whereas the latter two are associated with the directly allowed transition.[29,33] In addition, Mott-Schottky analysis indicated that the flat band potentials (E_{fb}) of CuO, Cu_2O, and $CuFeO_2$ are 0.574, 0.824, and 0.694 V_{SCE}, respectively (1.2, 1.45, and 1.32 V_{RHE}, respectively) (Fig. S14). On the basis of the determined E_g and E_{fb} values, the conduction bands (cb) and valence bands (vb) of semiconductors were estimated and compared to the redox potentials of CO_2 and water (Fig. S15a). According to the band diagram, irradiated $CuFeO_2$ and CuO (even Cu_2O as well) are capable of reducing CO_2 to formate, whereas oxygen evolution would be very difficult, particularly with CuO, due to an ~200 mV overpotential requirement for O_2 evolution when wired to a Pt anode. As shown in Fig. S12, E_{cell}s of CuO-Pt and $CuFeO_2$-Pt couples initially increased to ~120 mV and then decreased to 5 mV. The former couple was more effective in producing formate, likely due to the high E_{cb} level of CuO and/or inhibition of unwanted internal charge recombination at $CuFeO_2$. However, the production of oxygen was trace with both couples. Although O_2 can be produced with $CuFeO_2$ due to low E_{vb}, charge recombination appeared to inhibit water oxidation. However, such recombination should be inhibited upon junction with CuO (Fig. S15b). With $CuFeO_2$/CuO, photogenerated electrons at high E_{cb} of $CuFeO_2$ can migrate to CuO, whereas those at low E_{cb} can trap photogenerated holes at CuO. The holes generated at CuO could not oxidize water effectively and hence are desired to be extinguished. Through this internal recombination, the high-energy holes generated at $CuFeO_2$

are more available for water oxidation. Incident photon-to-current efficiency (IPCE) measurement further indicated that charge separation efficiency is enhanced by creating the heterojunction structure (Fig. S16). CuO exhibited an IPCE of 3 ~ 10% in the wavelength range between 400 and 800 nm, whereas the IPCE values of $CuFeO_2$ and Cu_2O were smaller than 6 and 4%, respectively, in the same wavelength range. However, the IPCE value of $CuFeO_2$/CuO was ~28% at 400 nm and significantly higher in the long wavelength range.

Conclusions

In summary, this study has demonstrated that $CuFeO_2$/CuO can photoelectrochemically reduce CO_2 to formate at high selectivity and efficiency while simultaneously driving the oxidation of water to molecular oxygen without any external bias under circumneutral pH. This stand-alone system operates over 1 week with continued production of formate. The components of this p-type material are earth-abundant and inexpensive, and the fabrication process of the material is straightforward with reproducibility and scalability in common laboratories.

Acknowledgments

The authors thank the National Research Foundation for the Global Research Network Program (NRF-2014S1A2A2027802) and the Space Core Technology Development Program (NRF-2014M1A3A3A02034875), Korea. In addition, we are grateful to the Korea Center for Artificial Photosynthesis (KCAP) (No. 2009-0093880), the Korea CCS R&D Center (KCRC) (No. 2014M1A8A1049354), and partly Samsung Advanced Institute of Technology, Samsung Electronics Co., LTD, for financial supports. W.C. is

grateful to Global Research Laboratory Program (2014K1A1A2041044), funded by the Korean government (MSIP). This publication was made possible by a grant from the Qatar National Research Fund under its National Priorities Research Program (Award number NPRP 7-865-2-320). H.P. is grateful to Dr. Sonjong Hwang at the Solid State NMR Facility, California Institute of Technology, Pasadena, CA, for discussion of NMR data.

References

1. S. Bensaid, G. Centi, E. Garrone, S. Perathoner and G. Saracco, *ChemSusChem*, 2012, **5**, 500-521.
2. M. R. Hoffmann, J. A. Moss and M. M. Baum, *Dalton Trans.*, 2011, **40**, 5151-5158.
3. R. K. Yadav, J.-O. Baeg, G. H. Oh, N.-J. Park, K.-j. Kong, J. Kim, D. W. Hwang and S. K. Biswas, *J. Am. Chem. Soc.*, 2012, **134**, 11455-11461.
4. M. Halmann, *Nature*, 1978, **275**, 115-116.
5. B. A. Parkinson and P. F. Weaver, *Nature*, 1984, **309**, 148-149.
6. H. Park, H.-H. Ou, A. J. Colussi and M. R. Hoffmann, *J. Phys. Chem. A*, 2015, **119**, 4658-4666.
7. M. Azuma, K. Hashimoto, M. Hiramoto, M. Watanabe and T. Sakata, *J. Electrochem. Soc.*, 1990, **137**, 1772-1778.
8. S. K. Choi, U. Kang, S. Lee, D. J. Ham, S. M. Ji and H. Park, *Adv. Energy Mater.*, 2014, **4**, 1301614.
9. J. Liu, R. Cazelles, Z. P. Chen, H. Zhou, A. Galarneau and M. Antonietti, *Phys. Chem. Chem. Phys.*, 2014, **16**, 14699-14705.
10. W. Kim, G. Yuan, B. A. McClure and H. Frei, *J. Am. Chem. Soc.*, 2014, **136**, 11034-11042.
11. T. Arai, S. Sato, T. Kajino and T. Morikawa, *Energy Environ. Sci.*, 2013, **6**, 1274-1282.
12. W. Kim, T. Seok and W. Choi, *Energy Environ. Sci.*, 2012, **5**, 6066-6070.
13. K. W. Frese and D. Canfield, *J. Electrochem. Soc.*, 1984, **131**, 2518-2522.
14. R. Hinogami, Y. Nakamura, S. Yae and Y. Nakato, *J. Phys. Chem. B*, 1998, **102**, 974-980.
15. C. W. Li and M. W. Kanan, *J. Am. Chem. Soc.*, 2012, **134**, 7231-7234.
16. G. Ghadimkhani, N. R. de Tacconi, W. Chanmanee, C. Janaky and K. Rajeshwar, *Chem. Commun.*, 2013, **49**, 1297-1299.
17. X. Q. An, K. F. Li and J. W. Tang, *ChemSusChem*, 2014, **7**, 1086-1093.
18. A. D. Handoko and J. W. Tang, *Int. J. Hydrog. Energy*, 2013, **38**, 13017-13022.
19. C. G. Read, Y. Park and K. S. Choi, *J. Phys. Chem. Lett.*, 2012, **3**, 1872-1876.
20. J. Gu, A. Wuttig, J. W. Krizan, Y. A. Hu, Z. M. Detweiler, R. J. Cava and A. B. Bocarsly, *J. Phys. Chem. C*, 2013, **117**, 12415-12422.
21. K. P. Kuhl, E. R. Cave, D. N. Abram and T. F. Jaramillo, *Energy Environ. Sci.*, 2012, **5**, 7050-7059.

22. E. Mugnier, A. Barnabe and P. Tailhades, *Solid State Ion.*, 2006, **177**, 607-612.
23. A. Bak, W. Choi and H. Park, *Appl. Catal. B*, 2011, **110**, 207-215.
24. T. Reda, C. M. Plugge, N. J. Abram and J. Hirst, *Proc. Natl. Acad. Sci. U. S. A.*, 2008, **105**, 10654-10658.
25. Z. Chen, H. N. Dinh and E. Miller, *Photoelectrochemical Water Splitting: Standards, Experimental Methods, and Protocols*, Springer, 2013.
26. S. K. Choi, W. Choi and H. Park, *Phys. Chem. Chem. Phys.*, 2013, **15**, 6499-6507.
27. T. H. Jeon, W. Choi and H. Park, *Phys. Chem. Chem. Phys.*, 2011, **13**, 21392-21401.
28. H. W. Jeong, T. H. Jeon, J. S. Jang, W. Choi and H. Park, *J. Phys. Chem. C*, 2013, **117**, 9104-9112.
29. A. Derbal, S. Omeiri, A. Bouguelia and M. Trari, *Int. J. Hydrog. Energy*, 2008, **33**, 4274-4282.
30. J. Liu and M. Antonietti, *Energy Environ. Sci.*, 2013, **6**, 1486-1493.
31. K. Nakaoka, J. Ueyama and K. Ogura, *J. Electrochem. Soc.*, 2004, **151**, C661-C665.
32. F. A. Benko and F. P. Koffyberg, *J. Phys. Chem. Solids*, 1987, **48**, 431-434.
33. S. Omeiri, B. Bellal, A. Bouguelia, Y. Bessekhouad and M. Trari, *J. Solid State Electrochem.*, 2009, **13**, 1395-1401.

Supporting Information

Description on materials and methods

Scheme S1

Figs. S1 to S16

Figure Captions

Fig. 1. Surface characterization of $CuFeO_2$/CuO, CuO, $CuFeO_2$, and Cu_2O films electrodeposited on FTO for 2 h followed by calcinations under air or Ar atmospheres (see text and *Supporting Information* for detailed synthetic conditions): (a) XRD (+ originating from FTO); (b) XPS Cu2p bands (inset: Fe2p bands); (c) cross-sectional TEM images of $CuFeO_2$/CuO (see *Supporting Information* for other images); (d) EDX elemental mapping for the cross-section of $CuFeO_2$/CuO (green: Sn, blue: Cu, red: Fe).

Fig. 2. (a) Comparison of light-chopped linear sweep voltammograms for $CuFeO_2$/CuO, $CuFeO_2$, and CuO electrodes in CO_2-purged aqueous bicarbonate (0.1 M) solution. (b) Time-profiled formate productions with $CuFeO_2$/CuO electrodes at +0.15 V_{RHE} in bicarbonate (0.1 M) solutions purged with CO_2 or N_2 (PEC-1). (c) Comparison of time-profiled formate productions with open-circuited $CuFeO_2$/CuO, $CuFeO_2$, and CuO, and Cu_2O electrodes in CO_2-purged bicarbonate (0.1 M) solution (PEC-2). No potential biases were applied, and only open-circuit potentials (E_{ocp}) were recorded with a potentiostat during irradiation. (d) Time-profiled changes in cell voltage (E_{cell}), simultaneous production of formate, and solar-to-formate (STF) energy conversion efficiencies with wired $CuFeO_2$/CuO and Pt foil couples in CO_2-purged bicarbonate (0.1 M) solutions (PEC-3 and 4). In this two-electrode system, the $CuFeO_2$/CuO and Pt electrodes faced with a distance of ~ 3 mm, and E_{cell} was recorded using a potentiostat (solid blue line and filled symbols; PEC-3) or a multimeter (crossed blue line and open symbols; PEC-4). (e) Changes in E_{cell} and formate production with a wired $CuFeO_2$/CuO and Pt couple in CO_2-purged bicarbonate

(0.1 M) solutions (PEC-4). A simulated light (AM 1.5; 100 $mW \cdot cm^{-2}$) irradiated sample electrodes through FTO. See Scheme S1 in the *Supporting Information* for PEC-1, 2, -3, and -4 setups.

Fig. 3. (a) Time-profiled changes in potential of $CuFeO_2$/CuO (red and blue solid lines), production of formate (open symbols), and faradaic efficiency (closed symbols) under constant current (red circles: –0.2 mA; blue squares: –0.3 mA) with a three-electrode system in CO_2-purged bicarbonate (0.1 M) solution (PEC-1). (b) Oxygen evolution with a wired $CuFeO_2$/CuO and Pt foil couple (PEC-4) in ^{18}O-labeled water ($H_2{}^{18}O$, 20 vol. % in H_2O) as a solvent in which bicarbonate salt was dissolved (0.1 M) and CO_2 gas was purged for over 1 h prior to irradiation. The relative abundance of $^{32}O_2$ and $^{34}O_2$ was compared. A simulated light (AM 1.5G; 100 $mW \cdot cm^{-2}$) irradiated $CuFeO_2$/CuO through FTO.

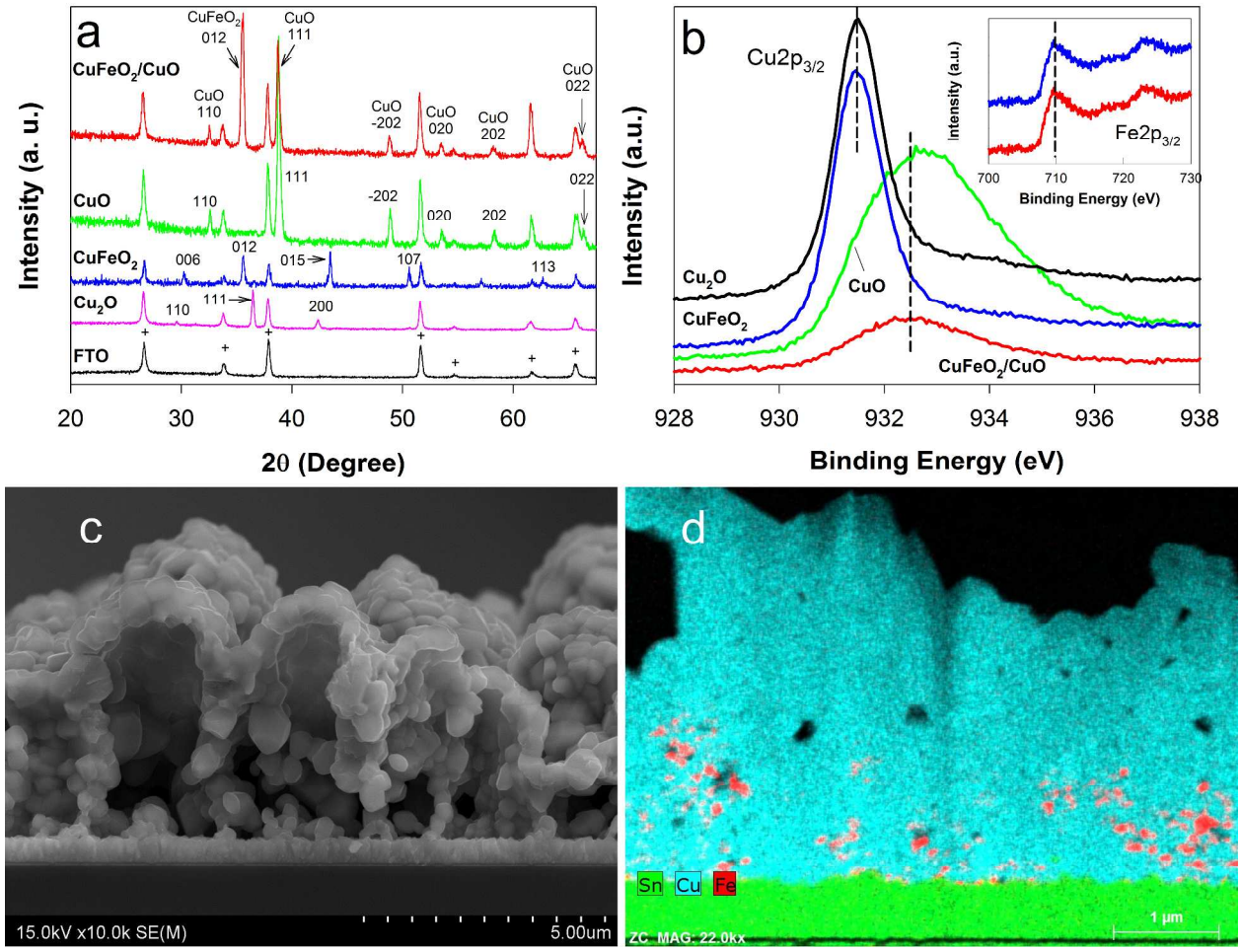

Figure 1. Kang et al.

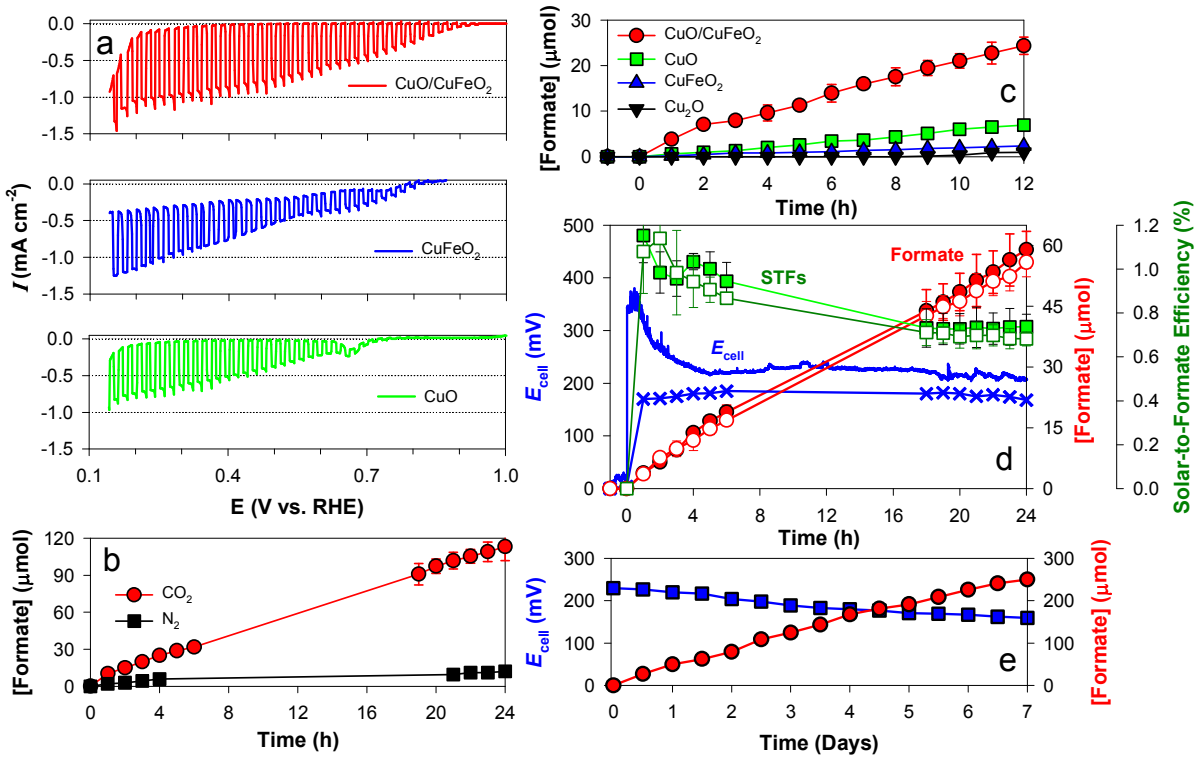

Figure 2. Kang et al.

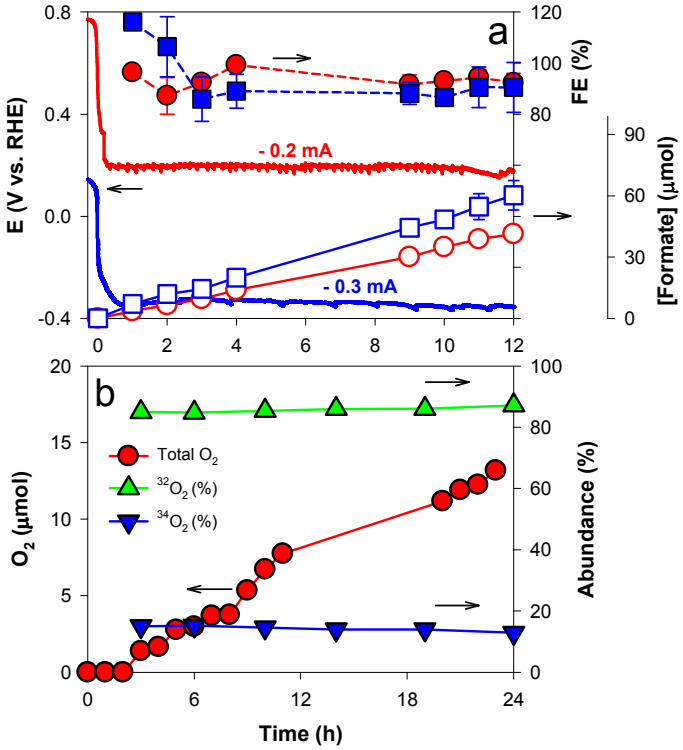

Figure 3. Kang et al.